

Supporting Information

Polar nano-region structure in the oxynitride perovskite LaTiO_2N

Jun-ichi Yamaura,^{*a} Sachiko Maki,^a Takashi Honda,^b Yoshio Matsui,^c Alfian Noviyanto,^c Toshiya Otomo,^b
Hitoshi Abe,^b Youichi Murakami,^{a,b} and Naoki Ohashi^{a,c}

^aMaterials Research Centre for Element Strategy, Tokyo Institute of Technology, Yokohama, Kanagawa 226-8503, Japan.

^bCondensed Matter Research Centre, Institute of Materials Structure Science, High Energy Accelerator Research Organization (KEK),
Tsukuba, Ibaraki 305-0801, Japan.

^cNational Institute for Materials Science, Tsukuba, Ibaraki 305-0044, Japan.

Table of contents

1. Materials and Methods
2. Sample characterization by electron microscope
3. Crystallographic parameters
4. Comparison between *Imma* and *I-1* models
5. Subgroups of *Imma* space group
6. PDF analysis in $1.6 < r < 20 \text{ \AA}$
7. O/N ordered model

1. Materials and Methods

Powder samples of LaTiO_2N were prepared from $\text{La}_2\text{Ti}_2\text{O}_7$ by ammonolysis reaction under NH_3 gas flow at 973 K for 60 h.² Synchrotron XRD measurements were carried out at 300 K at the Photon Factory (PF) BL-8A beamline at the High Energy Accelerator Research Organization (KEK). Two-dimensional images were obtained using a diffractometer with curved imaging plate (Rigaku R-AXIS), where the wavelength was set at $\lambda = 0.999175 \text{ \AA}$ to identify small peak splittings. The exposed images were integrated to yield 2θ -intensity data, and crystal structure was analyzed for 493 reflections using Rietveld method on the RIETAN-FP program.³² The electron density distribution was determined by a maximum-entropy method (MEM) based pattern fitting using RIETAN-FP and PRIMA programs.³³

To investigate the local structure, we carried out EXAFS and PDF analysis. La *K*-edge transmission EXAFS of the LaTiO_2N powder sample was measured at the PF-AR (advanced ring) NW-10A beamline at KEK. EXAFS oscillations and *R*-space magnitude of the Fourier transformation were extracted from the raw data using the Athena program.³⁴ The *R*-space data were fitted to the theoretical signals calculated by FEFF8 code using IFEFIT on the Artemis platform.³⁴ The PDF data from neutron total scattering were measured from ~0.45 g LaTiO_2N powder sample using the BL21 High Intensity Total Diffractometer (NOVA)³⁶ at the Materials and Life Science Experimental Facility (MLF) pulsed neutron source, Japan Proton Accelerator Research Complex (J-PARC). The sample was placed into a V96.4-Ni3.6 cell with an inner diameter of 6 mm ϕ . The structure factor $S(Q)$ was extracted from the data with corrections to instrument background, incident neutron spectrum, absorption, incoherent scattering, and multiple scattering. The PDF $G(r)$ was obtained through the Fourier transformation of $S(Q)$ and analyzed using the PDFgui program³⁷ with a *Q*-range of $1 < Q < 30 \text{ \AA}^{-1}$.

2. Sample characterization by electron microscope

The LaTiO_2N samples were characterized by using scanning and transmission electron microscopes (SEM and TEM). The Selected area electron diffraction (SAED) patterns as shown in Fig. S1c and e identify the extinction conditions with $h00$: $h = \text{odd}$, $0k0$: $k = \text{odd}$, $00l$: $l = \text{odd}$, $hk0$: $h+k = \text{odd}$, $0kl$: $k+l = \text{odd}$, and hkl : $h+k+l = \text{odd}$, implying that the symmetry holds the I -centered lattice. However, we could not identify the presence of a -glide plane, *i.e.* the reflection condition $hk0$: $h = \text{even}$, because of the domains of rotational twin.

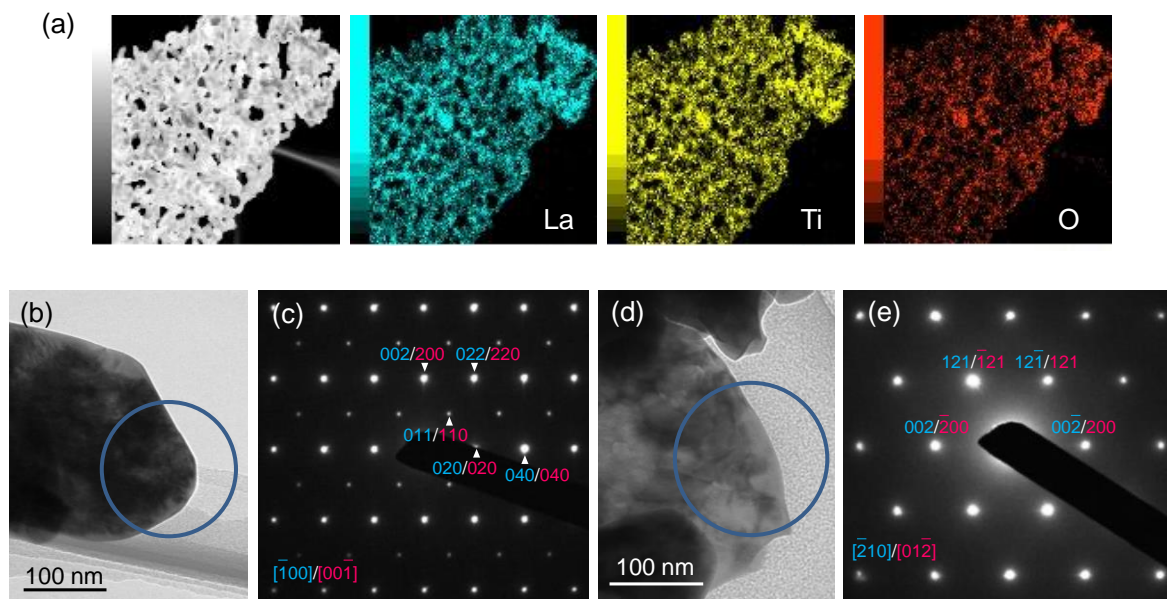


Fig. S1 (a) SEM image and its element mapping on La L -, Ti K -, and O K -edges from energy dispersive X-ray spectrometry, indicating the homogeneous distributions of components. TEM bright-field (b, d) and lattice images (c, e). (c, e) SAED patterns for the $[-100]/[00-1]$ and $[-210]/[01-2]$ orthorhombic zone axes. The patterns are indistinguishable from the domains of rotational twin. The SAED patterns with orthorhombic indices identify the extinction conditions with $h00$: $h = \text{odd}$, $0k0$: $k = \text{odd}$, $00l$: $l = \text{odd}$, $hk0$: $h+k = \text{odd}$, $0kl$: $k+l = \text{odd}$, and hkl : $h+k+l = \text{odd}$.

3. Crystallographic parameters

Table S1 Crystallographic data for LaTiO₂N at 300 K. The structural parameters are refined with the *Imma* (orthorhombic #74, $Z = 4$) space group for XRD and PDF1 ($8 < r < 20$ Å) and *Ima2* (orthorhombic #46, $Z = 4$) for PDF2 ($1.6 < r < 8$ Å). Atomic positions and Wyckoff letters (W. L.) are also shown.²⁷ The cell settings of *Imma* and *Ima2* are related by $(\mathbf{a}, \mathbf{b}, \mathbf{c})_{Imma} = (\mathbf{c}, \mathbf{a}, \mathbf{b})_{Ima2}$.

Atom	W. L.	x	y	z	U_{iso} (10^{-3} Å ²)
XRD; <i>Imma</i> , $a = 5.57182(6)$, $b = 7.87509(8)$, $c = 5.60295(5)$ Å, $R_{wp} = 2.6\%$, $R_e = 0.70\%$, $R_I = 1.6\%$					
La	4e	0	1/4	0.014(4)	5.79(5)
Ti	4b	0	0	1/2	5.92(13)
O1/N1	4e	0	1/4	0.5790(9)	9.4(6)
O2/N2	8g	1/4	0.0349(4)	1/4	9.4
PDF1; <i>Imma</i> , $a = 5.5545(2)$, $b = 7.8626(4)$, $c = 5.6060(3)$ Å, $R_{wp} = 9.4\%$					
La	4e	0	1/4	0.002(2)	4.19(2)
Ti	4b	0	0	1/2	5.26(4)
O1/N1	4e	0	1/4	0.5625(1)	5.75(2)
O2/N2	8g	1/4	0.03399(5)	1/4	5.75
PDF2; <i>Ima2</i> , $a = 7.8660(14)$, $b = 5.5984(14)$, $c = 5.5618(9)$ Å, $R_{wp} = 11.6\%$					
La	4b	1/4	0.0050(13)	0	6.59(7)
Ti	4a	0	1/2	0.0233(24)	4.90(10)
O1/N1	4b	1/4	0.5688(1)	-0.0059(21)	7.35(3)
O2/N2	8c	0.03140(5)	0.2559(1)	0.2729(14)	7.35

4. Comparison between *Imma* and *I-1* models

We consider our *Imma* result and the previous *I-1* model by Clarke *et al.*² Table S2 gives their lattice parameters and atomic positions. Our model was transformed to *I-1* setting without any refinement. We note that those positions are quite similar to each other. Fig. S2 plots the X-ray pattern employed in Fig. 1 and the calculated profiles from our (magenta) and *I-1* (blue) structures. The profiles in *I-1* model is also quite similar to that in our model without any broadening from orthorhombic symmetry except for only slightly better fitting than our model. As pointed by the average and local structures sections, the difference between the observed and calculated profiles in 044 and 440 reflections arises from losing the inversion symmetry in nanoscale. Therefore, we advocate that the previous *I-1* structure is indeed regarded as *Imma* in view of average structure.

Table S2 Lattice parameters and atomic positions of our and Clarke *et al.* (Italic) structures for LaTiO₂N.

Atom	W. L.	<i>x</i>	<i>y</i>	<i>z</i>
Our data: <i>I-1</i> from <i>Imma</i> , <i>a</i> = 5.60295(5), <i>b</i> = 7.87509(8), <i>c</i> = 5.57182(6) Å, <i>α</i> = <i>β</i> = <i>γ</i> = 90°				
Clarke <i>et al.</i> ² : <i>I-1</i> , <i>a</i> = 5.6097(1), <i>b</i> = 7.8719(2), <i>c</i> = 5.5752(1) Å, <i>α</i> = 90.199(2), <i>β</i> = 90.154(3), <i>γ</i> = 89.988(8)°				
La	4 <i>i</i>	0.514(4) <i>0.4989(3)</i>	0.25 <i>0.2516(7)</i>	0 <i>0.0010(8)</i>
Ti1	2 <i>e</i>	0 <i>0</i>	0 <i>0</i>	0 <i>0</i>
Ti2	2 <i>g</i>	0 <i>0</i>	0.5 <i>0.5</i>	0 <i>0</i>
O1/N1	4 <i>i</i>	-0.0790(9) <i>-0.0620(2)</i>	0.25 <i>0.2495(8)</i>	0 <i>-0.0006(9)</i>
O2A/N2A	4 <i>i</i>	0.25 <i>0.260(1)</i>	0.0349(4) <i>0.0358(4)</i>	0.25 <i>0.243(1)</i>
O2B/N2B	4 <i>i</i>	0.25 <i>0.255(1)</i>	0.4651(4) <i>0.4730(4)</i>	0.75 <i>0.757(1)</i>

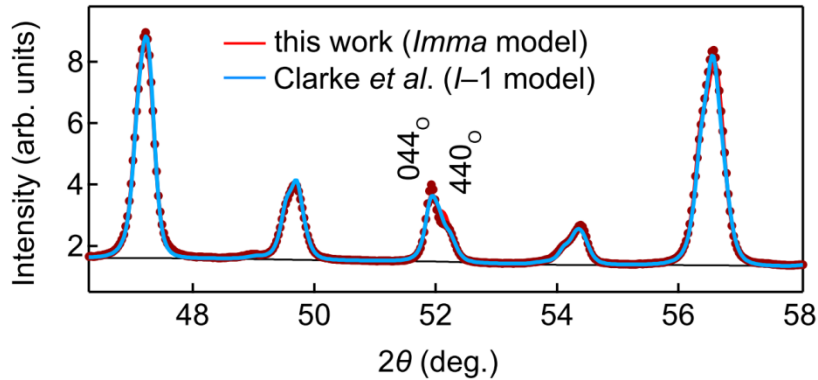


Fig. S2 X-ray diffraction pattern and the calculated profiles from our (magenta) and Clarke *et al.* *I-1* (blue) structures. Only the lattice parameters were refined in the *I-1* model.

5. Subgroups of *Imma* space group

We examined symmetry lowering on the basis of group-subgroup relations, accounting for possible orthorhombic space groups: non-centrosymmetric *Im2b* (*Ima2* in standard setting), *I2mb* (*Ima2*), *Imm2*, *I2₁2₁2₁*, and centrosymmetric *Pnma*, *Pmnb* (*Pnma*), *Pnmb* (*Pmna*), *Pmna*, *Pnna*, *Pnmb* (*Pnna*), *Pnma*, *Pmmb* (*Pmma*) among the maximal non-isomorphic subgroups of the *Imma*.⁵ The electron diffraction exhibited that the symmetry holds the *I*-centered lattice. We could not succeed to measure the SAED pattern for the [00-1] orthorhombic zone axis to identify the presence of *a*-glide axis because of the indistinguishable domains. However, we can narrow down the above candidates of subgroups from the XRD result. The elongated electron density of XRD implies the polar shift along the *a*-axis in view of average structure. The *I2mb*, *Im2b*, and *Imm2* involve the polarization along the respective *a*, *b*, and *c*-axes, and *I2₁2₁2₁* is non-polar space group without inversion symmetry. Therefore, *I2mb* (*Ima2*) are uniquely determined so as to satisfy the XRD and TEM results.

6. PDF analysis in $1.6 < r < 20 \text{ \AA}$

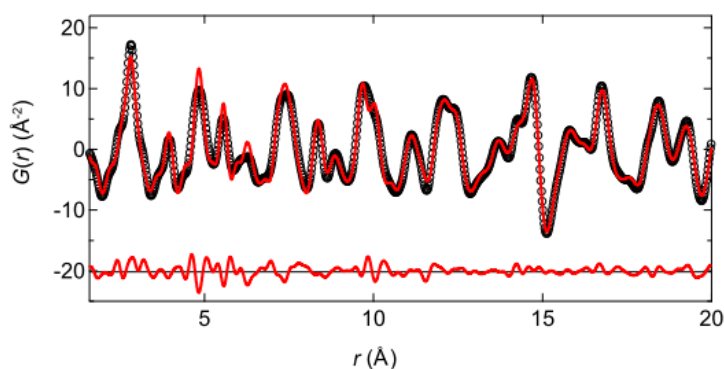


Fig. S3 PDF data (black circles) for LaTiO_2N at 300 K in the range $1.6 < r < 20 \text{ \AA}$. The red line is calculated from refinements using the centrosymmetric *Imma* model ($R_{\text{wp}} = 15.9\%$). The lower curve is the difference profile between the experimental data and the calculated patterns.

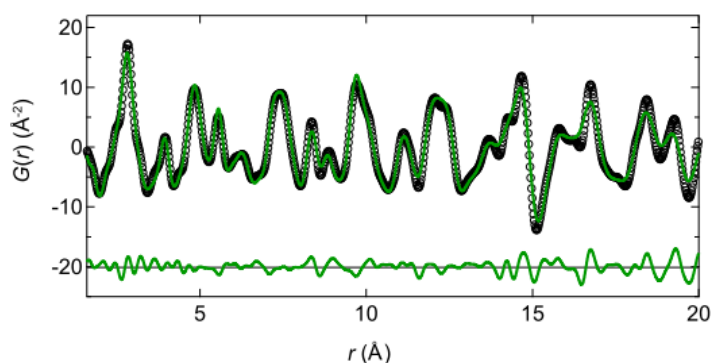


Fig. S4 PDF data (black circles) for LaTiO_2N at 300 K in the range $1.6 < r < 20 \text{ \AA}$. The green line is plotted from the fixed *Im2* model for short-range ($1.6 < r < 8 \text{ \AA}$) ($R_{\text{wp}} = 18.8\%$). The lower curve is the difference profile between the experimental data and the calculated patterns.

7. O/N ordered model

In AMO_2N materials, two classifications exist in the placement of O and N atoms at the six vertices of the MO_4N_2 octahedron: either two N atoms occupy opposite vertices in *trans*-order, or neighboring vertices in *cis*-order. We initially refine the structural parameters for representative *trans*- and *cis*-order models as illustrated in Fig. S5a. The structure refinements were started from the O/N disordered *Ima2* structure. The atomic positions were constrained by *Ima2* symmetry, and the parameters of $z(\text{O})$ and $z(\text{N})$ along the polar axis were constrained to common values. The final values of R_{wp} are described in Fig. S5a. While the *trans*-ordered models led to little refinement, the *cis2*, *cis3*, and *cis4* models delivered significant improvements as seen in Fig. S5b, suggesting that *cis*-ordering is a feasible O/N ordered state in the compound. In oxynitrides, the stronger covalency of N atoms has been considered to cause off-center displacement of the metal atoms.^{39,A1,A2} Based on the criteria, the *cis3* model is favored as the O/N ordering pattern as it accounts for the observed polar shift along the *c*-axis. However, one issue reported in the literature is that bulk *cis*-ordering is associated with an anti-polar state.³⁹ In our study, since the polar region emerges below 8 Å, a size effect may affect polarization in conjunction with *cis*-ordering. To ensure the above findings, further study is required on the O/N ordering through the NQR and polarized photoemission spectra that enable to visualize the anion ordering.

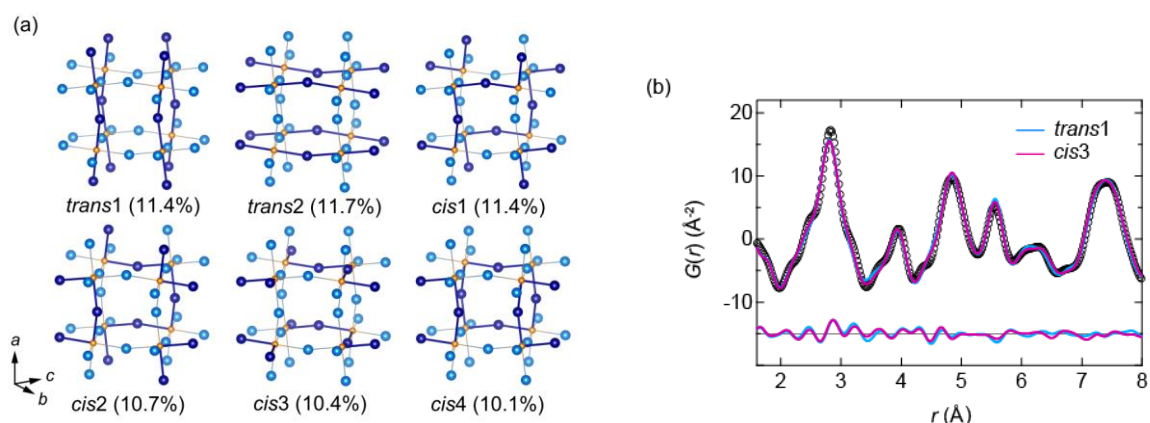


Fig. S5 (a) O/N ordered models for the six vertices of the TiO_4N_2 octahedron, together with their weighted R -factors. The Ti, O, N atoms are represented by orange, blue, and indigo balls. The two N atoms occupy opposite sites in *trans*-order and neighboring sites in *cis*-order on the octahedron. Crystallographic axes are set to the *Ima2* structure. (b) PDF data (black circles) for the range $1.6 < r < 8$ Å. Top plots represent *trans1* (blue line) and *cis3* (magenta line) models. Lower curves are the difference profiles between the experimental and the calculated data.

References

- A1. M. Yang, J. Oro-Sole, J. A. Rodgers, A. B. Jorge, A. Fuertes and J. P. Attfield, *Nat. Chem.*, 2011, **3**, 47–52.
A2. S. Ninova and U. Aschauer, *J. Mater. Chem. A*, 2017, **5**, 11040–11046.